Nano Research

Open Access

Research Article

# Non-hand-worn, load-free VR hand rehabilitation system assisted by deep learning based on ionic hydrogel

Pengcheng Zhu[§], Mengjuan Niu[§], Siyang Liang, Weiqi Yang, Yitao Zhang, Ke Chen, Zhifeng Pan, and Yanchao Mao

*Key Laboratory of Materials Physics of Ministry of Education, School of Physics, Zhengzhou University, Zhengzhou 450001, China*
*[§] Pengcheng Zhu and Mengjuan Niu contributed equally to this work.*

**Cite this article:** *Nano Research*, **2025**, *18*, 94907301. https://doi.org/10.26599/NR.2025.94907301

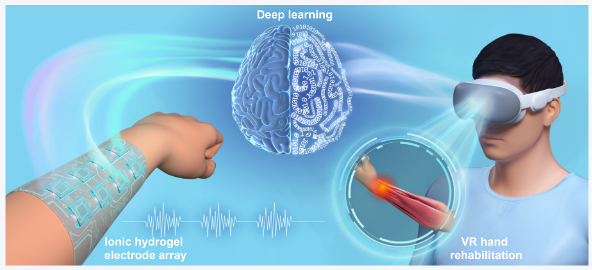


**ABSTRACT:** Many individuals suffer from stroke, osteoarthritis, or accidental hand injuries, making hand rehabilitation greatly significant. The current hand rehabilitation therapy requires repetitive task-oriented hand exercises, relying on exoskeleton mechanical gloves integrated with different sensors and actuators. However, these conventional mechanical gloves require wearing heavy mechanical components that need weight-bearing and increase hand burden. Additionally, these devices are usually structurally complex, complicated to operate, and require specialized medical institutions. Here, a Virtual Reality (VR) hand rehabilitation system is developed by integrating deep-learning-assisted electromyography (EMG) recognition and VR human-machine interfaces (HMIs). By applying a wet-adhesive, self-healable, and conductive ionic hydrogel electrode array assisted by deep learning, the system can realize 14 Jebsen hand rehabilitation gestures recognition with an accuracy of 97.9%. The recognized gestures further communicate with the VR platform for real-time interaction in a virtual scenario to accomplish VR hand rehabilitation. Compared with present hand rehabilitation devices, the proposed system enables patients to perform immersive hand exercises in real-life scenarios without the need for hand-worn weights, and offers rehabilitation training without time and location limitations. This system could bring great breakthroughs for the development of a load-free hand rehabilitation system available in home-based therapy.

**KEYWORDS:** human-machine interfaces, virtual reality systems, electrophysiological monitoring, ionic hydrogels

## 1 Introduction

Nowadays numerous people suffer from stroke, osteoarthritis, or accidental hand injuries that cause severe hand dysfunction [1–4], making effective hand rehabilitation of great significance for patients to regain their normal lives [5–7]. Conventional rehabilitation therapy includes repetitive task-oriented hand exercises, which rely on exoskeleton mechanical gloves integrated with different sensors and actuators [8–11]. When patients with hand dysfunction perform various hand motions, the sensors of the exoskeleton glove measure joint angle and contact force of fingers, thus recognizing different gestures and making assessments for hand health conditions [12–14]. However, these conventional rehabilitation therapies require wearing bulky mechanical components, which needs weight-bearing and increases hand burden [15–17]. On the other hand, these hand rehabilitation devices are usually structurally complex, complicated to operate, and require treatment to be conducted in specialized medical institutions [18, 19]. In recent years, Virtual Reality (VR) based human-machine interfaces (HMIs) has emerged as a novel rehabilitation therapy for limb injury patients [20–22]. Since VR HMIs can engage patients in performing immersive repetitive goal-oriented hand motions that simulate real-life scenarios [23, 24]. It is also easy and fun to operate without time and location constraints. However, the current VR HMIs system still requires wearable mechanical devices [25–27], which similarly face issues such as increased hand burden and susceptibility to fatigue-related injuries. Therefore, it is highly desirable to develop a VR hand rehabilitation system available in home-based therapy without heavy wearable components.

Electrophysiological devices can collect biomedical electromyography (EMG) signals generated in muscles when performing different motions. These signals contain rich information about muscle activity which effectively reflects the intended motions [28, 29]. Applying stretchable conductive electrodes to seamlessly attach onto arm skin enables EMG signal

**Received:** December 24, 2024; **Revised:** February 11, 2025
**Accepted:** February 12, 2025

✉Address correspondence to ymao@zzu.edu.cn

acquisition generated by hand movements [4, 30–32], which could be used for gesture recognition without wearing weight-load gloves. However, these EMG electrodes face low recognition accuracy, because the acquired EMG signals are often complex and disordered due to muscle crosstalk [33], and superficial information such as frequency, intensity, and duration is insufficient to accurately recognize the diverse hand gestures in daily life. Although human-machine interfaces and robot control based on EMG signals collected by electrophysiological electrodes have been reported [34, 35], these typically rely on simple on-off signal triggers, making precise multi-gesture control difficult to achieve. Deep learning is a technology capable of extracting subtle and critical features from complex signals, with a distinct advantage in handling large datasets and classifying them [36–38]. After training on a substantial amount of known data, deep learning models can recognize and make accurate predictions on unknown input signals [39–41]. Combining deep learning to assist in gesture recognition based on EMG signals collected by stretchable electrophysiological electrodes, it is possible to achieve active interaction between hand motions and VR space without wearing bulky weights, holding great potential to develop a non-hand-worn, load-free VR hand rehabilitation system.

Herein, we developed a deep learning-assisted VR hand rehabilitation system based on hand motion EMG signals acquired by a wet-adhesive, self-healable, and conductive ionic hydrogel electrode array. The stretchable ionic hydrogel electrodes enable precise and stable acquisition of diverse electrophysiological signals with higher signal quality than those of commercial Ag/AgCl gel electrodes. An ionic hydrogel array was attached to the forearm skin to collect 6-channel EMG signals generated by 14 different Jebsen hand rehabilitation gestures, with 5 volunteers performing each gesture for 100 times. The resulting EMG data were used to train the constructed Convolutional Neural Network (CNN), achieving a recognition accuracy of 97.9% for the various Jebsen hand function gestures. Further, the recognized gestures can communicate with Unity platform in the VR system, achieving real-time VR rehabilitation training for Jebsen hand function tests. Compared to traditional rehabilitation devices, our VR rehabilitation system eliminates the need for hand-worn weights and offers the flexibility of immersive and precise rehabilitation training without constraints of time and location. This deep learning-assisted EMG-controlled VR hand rehabilitation system holds the potential to bring breakthroughs in rehabilitation therapy for patients with stroke and joint diseases.

## 2 Results and discussion

### 2.1 Schematic of hand motion recognition assisted by deep learning for VR hand rehabilitation and ionic hydrogel's structure

Figure 1(a) illustrates the schematic of VR hand rehabilitation, which is based on hand motion EMG recognition assisted by deep learning. In this system, multi-channel EMG signals generated by diverse hand motions are collected by an ionic hydrogel electrode array and processed by a trained CNN to recognize corresponding hand motions, which are then transmitted to VR Unity platform to synchronize the virtual hand movement. This setup enables the hand injury patient wearing a VR headset, to perform hand motions and experience real-time feedback in the virtual space, realizing VR hand rehabilitation. Figure 1(b) shows that the prepared ionic hydrogel comprises branched polyethylene imine

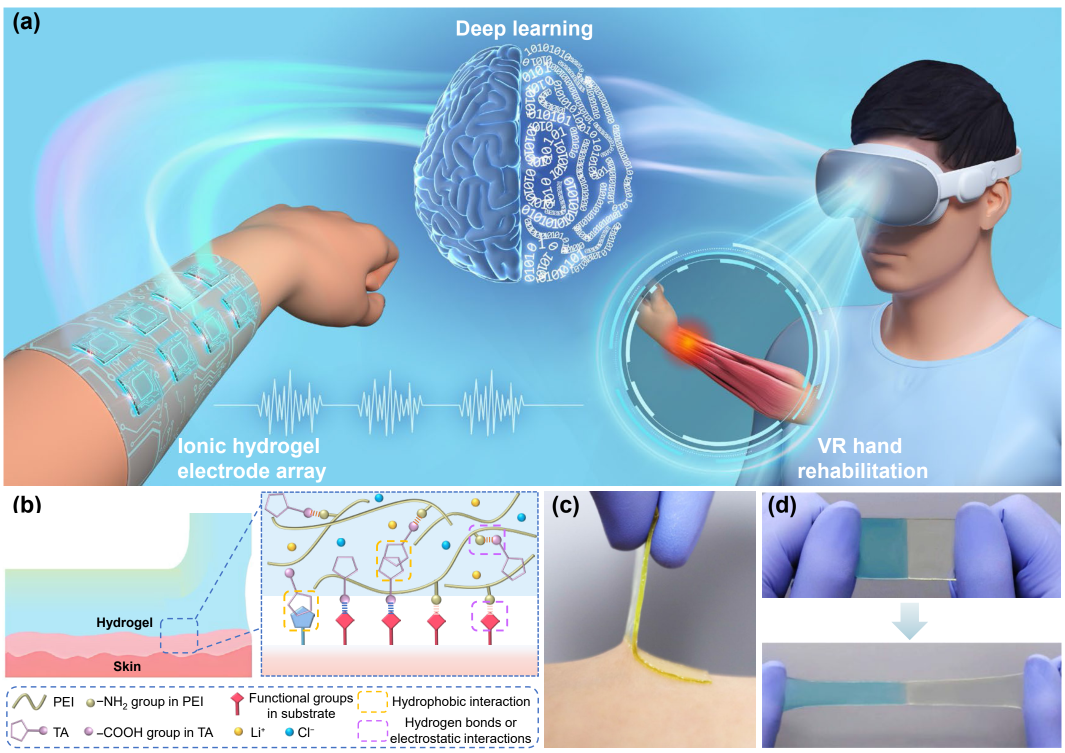


**Figure 1** Schematic of hand motion recognition achieved by deep learning for VR hand rehabilitation and basic structure of the ionic hydrogel. (a) Sketch of the deep learning-assisted EMG gesture recognition for VR hand rehabilitation. (b) Basic structure of the ionic hydrogel and its adhesive mechanism. (c) Photograph of the ionic hydrogel film showing its strong adhesion to human skin. (d) Photographs showing the ionic hydrogel's self-healing property.


清华大学出版社 Tsinghua University Press | SciOpen

(PEI), thioctic acid (TA), and LiCl. Branched PEI which contains rich amine with minimal steric hindrance, plays a crucial role in its complexation with TA. The amine groups of branched PEI allow for extensive electrostatic interactions with the carboxylic acid in TA. Additionally, the branched PEI structure can facilitate hydrophobic interactions between TA molecules, thereby enhancing the solubility of TA in aqueous solutions. The branched PEI and TA can thus easily form a coacervate-derived ionic hydrogel, the formation mechanism of the ionic hydrogel is depicted in Fig. S1 in the Electronic Supplementary Material (ESM). Adding LiCl can significantly increase the ionic hydrogel's conductivity since the branched PEI contains N atoms in its amino groups, which can solvate $Li^+$ ions due to the electron pair in the N nucleus's outermost layer. This allows ion transport between nitrogen sites, facilitating efficient transportation of $Li^+$ ions and greatly enhancing the ionic hydrogel's conductivity by providing abundant $Li^+$ transport channels [42]. When in contact with wet surfaces, the PEI/TA ionic hydrogel can repel the interfacial water and adhere tightly to the substrate's irregularities. The PEI's amine groups, along with the carboxyl groups in TA could have physical interactions such as hydrogen bonding and electrostatic interactions with functional groups on the substrate, resulting in strong adhesiveness. Figure 1(c) demonstrates the ionic hydrogel film's strong adhesion to human skin when it was peeling off. Meanwhile, Fig. 1(d) highlights the ionic hydrogel's excellent self-healing property. Thanks to the strong physical interactions between amino groups and carboxyl groups, such as electrostatic interaction and hydrogen bonding, TA can quickly entangle with the PEI chains and self-heal within one minute, regaining its original stretchability.

## 2.2 Electrical, mechanical, and adhesive properties of the ionic hydrogel

The ionic hydrogel exhibits high wet adhesion, conductivity, and self-healing properties, its comprehensive performances were evaluated across various parameters. Figure 2(a) presents the electrochemical impedance spectroscopy (EIS) plots of the ionic hydrogels prepared with different concentrations of LiCl, the ionic hydrogel impedance gradually decreases with the rising of the LiCl content. Figure 2(b) presents the ionic hydrogels' conductivity, calculated from the EIS plots through the equation $\sigma = L/SR$, where $R$ is the ionic hydrogel's bulk resistance which can be obtained from the intercept of the $X$-axis in EIS plots, $S$ is the effective area, and $L$ is the thickness of ionic hydrogel. It can be seen that the conductivity improved from 0.7 to 3.3 mS/cm as the LiCl content rose from 0.01 to 0.05 g/mL. Figure S2 in the ESM shows the contact impedance with human skin for the ionic hydrogel with a LiCl content of 0.02 g/mL, where the ionic hydrogel exhibits lower contact impedance compared with commercial Ag/AgCl gel electrodes within the range of $10^2$ to $10^5$ Hz, further proving the excellent conductivity of the ionic hydrogel when using as an electrophysiological electrode. The ionic hydrogels' mechanical performance with varying LiCl contents was also evaluated by the stress–strain curves, as shown in Fig. 2(c). The corresponding strain elongation of the ionic hydrogel as a function of LiCl content is presented in Fig. 2(d). The elongation of the ionic hydrogel greatly increased from 600% to 1060% when the LiCl content rose from 0 to 0.02 g/mL, with the Young's modulus decrease from 13.4 to 6.7 kPa (see Fig. S3 in the ESM). Further addition of LiCl up to

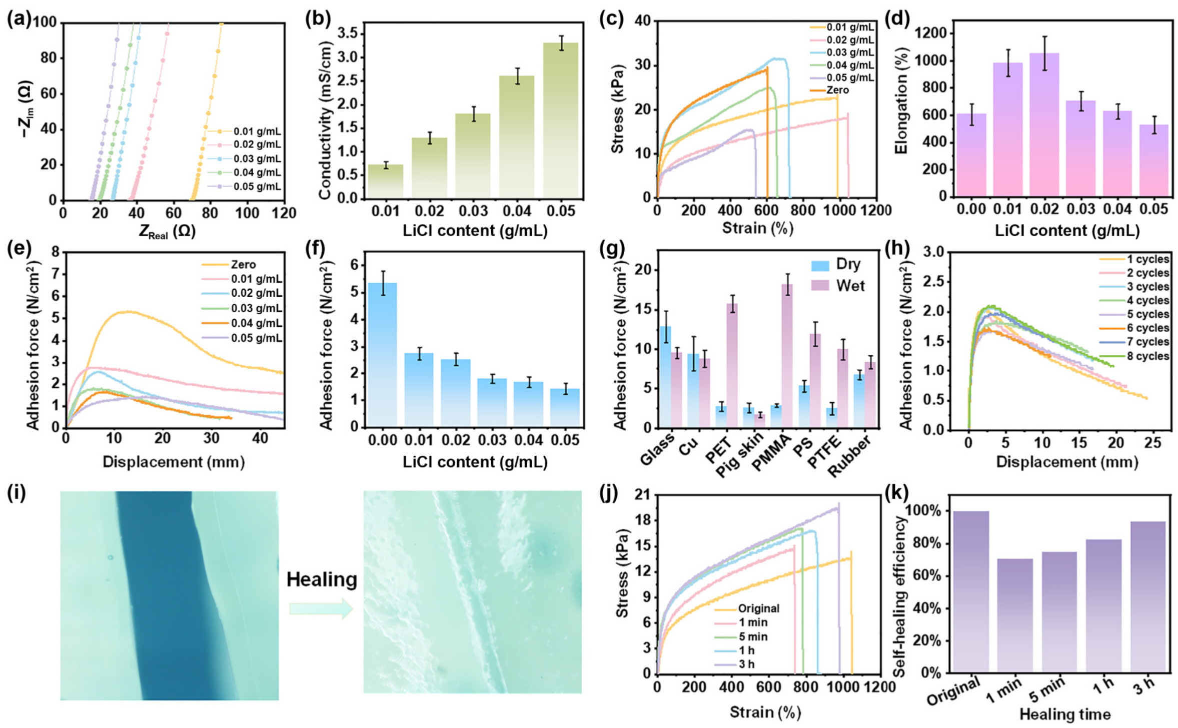


**Figure 2** Electrical, mechanical, and adhesive properties of the ionic hydrogel. (a) EIS plots of the ionic hydrogels with different contents of LiCl. (b) Conductivity of the ionic hydrogels with different contents of LiCl calculated from the EIS plots. (c) Stress–strain curves of the ionic hydrogels with different LiCl contents. (d) Strain elongation of the ionic hydrogels as a function of LiCl content. (e) Adhesion force curves of the ionic hydrogels with different LiCl contents to dry porcine skin. (f) Corresponding adhesion forces of the ionic hydrogels to dry porcine skin as a function of LiCl content. (g) Adhesion forces of the ionic hydrogel to different substrates in dry and wet conditions, including glass, Cu, PET, pig skin, PMMA, PS, PTFE, and rubber. (h) Adhesion force curves of the ionic hydrogel's repetitive adhesion test for 8 cycles. (i) Optical microscope images of the gap of the break ionic hydrogel before and after self-healing. (j) and (k) Stress–strain curves and self-healing efficiency of the original and self-healed ionic hydrogels with different healing times.

0.05 g/mL decreased the elongation to 530%, indicating the optimal stretchability of the ionic hydrogel at 0.02 g/mL of LiCl content. The introduction of LiCl enhances mechanical properties by shielding charges on the PEI chains, which enables the curling chains to extend, facilitating the creation of more entanglements between PEI and TA chains, and enhancing hydrogen bonds that serve as sacrificial bonds to dissipate energy during stretching [43]. The subsequent decrease in elongation can be attributed to excessive $Li^+$ ions disrupting the electrostatic interactions between PEI and TA chains. The ionic hydrogels' adhesive properties were further investigated by the lap shear test method (Fig. S4 in the ESM). Figure 2(e) shows the adhesion force curves of the ionic hydrogels with different LiCl contents to dry porcine skin. As the LiCl content increased from 0 to 0.05 g/mL, the maximum adhesion force showed a declining trend. Figure 2(f) summarizes the adhesion force, which decreased from 5.4 to 1.4 N/cm$^2$ with increased LiCl concentration, these adhesion forces are comparable to those recently reported adhesive hydrogels [44–47]. The decreased adhesion force may be attributed to weakened interactions between functional groups and the substrate induced by the incorporation of $Li^+$. Considering the balance between mechanical, electrical, and adhesive properties, the ionic hydrogel prepared with 0.02 g/mL of LiCl was chosen as the optimal sample for further testing. Then the ionic hydrogel's adhesion forces on multiple materials under dry and wet conditions were tested (Fig. 2(g)). The ionic hydrogel maintains excellent adhesion on eight types of materials under both dry and wet states, all exceeding 1.6 N/cm$^2$. In fact, for materials like polyethylene terephthalate (PET), polymethyl methacrylate (PMMA), and polytetrafluoroethylene (PTFE), wet adhesion was stronger than dry adhesion. This can be explained by the 1,2-dithiolanes and alkyl chains of ionic hydrogel forming hydrophobic interactions in the adhesion interface to exclude interfacial water and fill in the substrate's surface, ensuring high adhesion under wet conditions. This wet adhesion feature could guarantee good contact of the ionic hydrogel electrode with the skin under severe sweat conditions, ensuring stable electrophysiological signals acquisitions even during sports or outdoor activities. Reusability of the ionic hydrogel electrodes is essential for long-term health monitoring, so periodic adhesion and peeling experiments were conducted on porcine skin for 8 cycles to test the ionic hydrogel's repetitive adhesion, see Fig. 2(h). The detailed adhesion force as a function of adhesion cycles can be found in Fig. S5 in the ESM. The results show consistent adhesion forces (1.7–2.1 N/cm$^2$) throughout the adhesion cycles, demonstrating stable repetitive adhesion. Additionally, the adhesive force on porcine skin was tested over extended durations to evaluate the long-term adhesiveness, which exhibited a slight decrease from 2.1 to 1.7 N/cm$^2$ after 24 h of adhesion (Figs. S6 and S7 in the ESM). Given the frequent stress and deformation that electrodes endure during human motion, developing a self-healing ionic hydrogel that mimics the function of the skin is crucial for prolonged sensor life. Figure 2(i) shows an optical microscope image of the gap of the break ionic hydrogel. It can be observed that the gap nearly disappeared after self-healing, thanks to the strong physical interactions between PEI and TA polymer chains. Figures 2(j) and 2(k) present the stress–strain curves as well as the self-healing efficiency of the ionic hydrogels with different healing times. After 1 min, the ionic hydrogel's fracture interface can quickly rejoin, regaining its stretchability up to 730% with a self-healing efficiency of 70%. Extending the self-healing time to 3 h increased elongation to 970%, with an impressive self-healing efficiency of 93%. This highlights the almost complete recovery of mechanical properties due to the regain of electrostatic interactions and hydrogen bonds at fracture interface. Finally, the impedance of the ionic hydrogel on porcine skin after self-healing was evaluated (Fig. S8 in the ESM), showing negligible changes, further confirming the ionic hydrogel's durability and self-healing capabilities.

### 2.3 Electrophysiological signals monitoring of the ionic hydrogel electrode

Thanks to the superior wet adhesiveness and conductivity, the ionic hydrogel could function as a high-precision electrode for various electrophysiological signal acquisitions. The ionic hydrogel electrodes were adhered to different skin areas to monitor signals like electroencephalogram (EEG), electrocardiogram (ECG), and EMG. First, the ionic hydrogel electrodes were attached to two sides of the forehead to capture EEG signals under different mental states. Each state was recorded for 5 s with a 5-minute rest between every mental state. Figure 3(a) shows all raw EEG signals of the testing subject in mental states of thinking, eyes-closed relaxing, and eyes-open neutral state, which reveal distinguishable patterns for each mental state. The corresponding time-frequency spectrograms of different EEG signals in Fig. 3(b) further confirm these differences in frequency distribution. The fast Fourier transform (FFT) was extracted from all raw EEG signals to analyze the frequency characteristics, as shown in Fig. 3(c). The signal frequencies of thinking, eyes-closed relaxing, and eyes-open neutral states correspond to EEG wavebands at around 24, 10, and 3 Hz, respectively. These frequency activities align with cerebral activities reported in previous works [48–51], demonstrating the high accuracy of the ionic hydrogel electrode in capturing weak and mixed EEG signals. Next, the ionic hydrogel electrode was attached to the arms of a testing subject for acquiring ECG signals, with commercial Ag/AgCl gel electrode as a control. Except for static conditions, it is also of great significance to monitor ECG signals in sports scenarios such as running and jogging. Hence, a vibrator was used to simulate these conditions by generating vibrations at varying intensities, which is achieved by placing a vibrator on the arm at various distances from the electrodes (1 to 5 cm). Figure 3(d) shows that the ionic hydrogel electrodes provide clear and stable ECG signals under different vibration intensities, comparable to those from commercial electrodes. The signal-to-noise ratio (SNR) of the ECG signals acquired by ionic hydrogel electrodes and commercial electrodes were further analyzed (Fig. 3(e)). We can see that the SNR of ECG signals from ionic hydrogel electrode remained stable from 21.8 to 20.9 dB, whereas the SNR of commercial Ag/AgCl gel electrodes decreased significantly from 21.2 to 18.9 dB under the same condition, which is attributed to the ionic hydrogel electrode's superior adhesion and low contact impedance. High conductivity ensures the lower contact resistance of the ionic hydrogel electrode with human skin, as indicated in Fig. S2 in the ESM. While high adhesiveness keeps firm and stable contact with skin when the electrode is in vibration conditions. The ionic hydrogel electrodes were also tested for continuous ECG monitoring. Figure 3(f) shows continuous ECG signals of a young adult over 60 s with clear and stable waveforms. The corresponding heart rate was extracted to be around 78 bpm (Fig. S9 in the ESM), which is consistent with that of a commercial ECG monitor, demonstrating the reliability of the ionic hydrogel

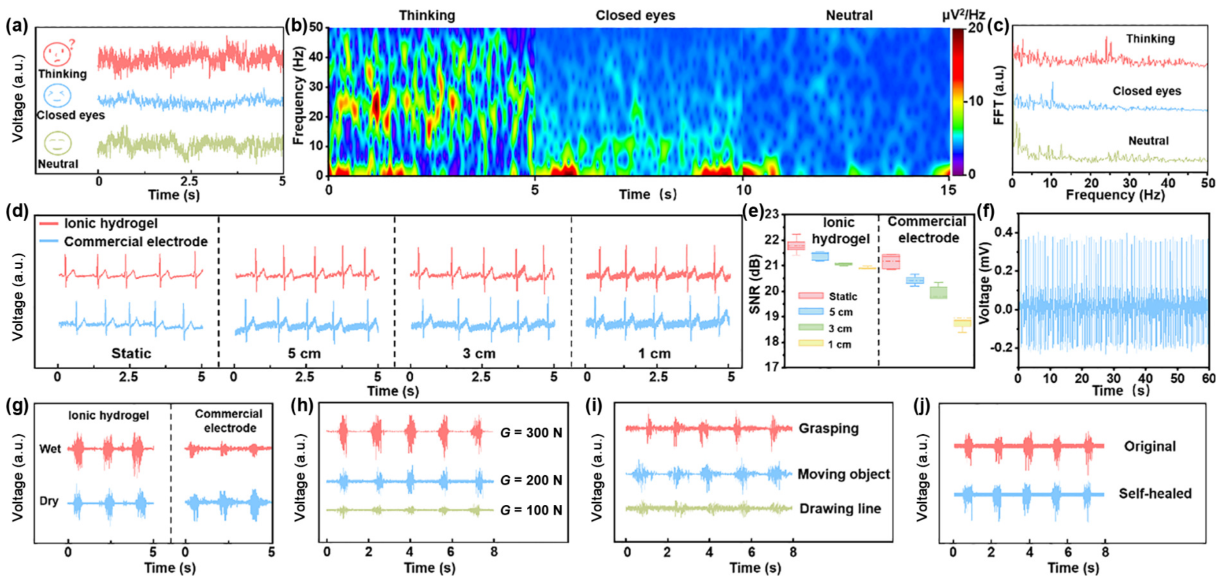


**Figure 3** Electrophysiological signals monitoring of the ionic hydrogel electrode. (a) Raw EEG signals of a testing subject in mental states of gritting teeth, blinking, and smiling. (b) Corresponding time-frequency spectrograms of different EEG signals. (c) FFT results extracted from the raw EEG signals. (d) ECG signals acquired by the ionic hydrogel and commercial Ag/AgCl gel electrodes under different vibration intensities. (e) Corresponding signal-to-noise ratio of the ECG signals acquired by ionic hydrogel and commercial electrodes. (f) Continuous ECG signals of a young man monitored by the ionic hydrogel for over 60 s. (g) EMG signals acquired by the ionic hydrogel during dry and sweaty skin conditions. (h) EMG signals acquired by the ionic hydrogel with varying clenching forces. (i) EMG signals acquired by the ionic hydrogel for different hand motions including grasping, moving objects, and drawing a line. (j) EMG signals from the ionic hydrogel in normal state and after its self-healing.

electrode. The detailed ECG waveform for one heartbeat is presented in Fig. S10 in the ESM, showing distinct P, Q, R, and T waves that deliver sufficient information for diagnostic purposes. After being stored in the ambient environment for 24 h, the ionic hydrogel could still work normally for ECG monitoring, as shown in Fig. S11 in the ESM, indicating good long-term stability of the hydrogel electrodes. Furthermore, due to its good wet adhesion ability, the ionic hydrogel electrode was employed to record EMG signals during sweat in exercise conditions. The ionic hydrogel electrodes were attached to a subject's forearm to acquire EMG signals of clenching a fist. Figure 3(g) compares the EMG signals of making a fist with the same power during dry and post-exercise sweat skin conditions. The EMG signals of the ionic hydrogel electrode under wet conditions show no degradation in signal quality compared to those in dry conditions. Whereas the EMG signals obtained from commercial Ag/AgCl gel electrode suffered significant signal degradation in sweat conditions. The ionic hydrogel electrode's ability to distinguish grip strength was tested by monitoring EMG signals at varying clenching forces from 100 to 300 N by using a grip dynamometer. Figure 3(h) shows that the EMG signal intensity accordingly increased with the rising clenching force. To explore the potential of the ionic hydrogel to differentiate various types of hand gestures, EMG signals were recorded by the ionic hydrogel electrodes for different hand motions, including grasping objects, moving objects, and drawing a line. Figure 3(i) shows distinct EMG waveform patterns for each gesture, demonstrating the ionic hydrogel's suitability for EMG-based gesture recognition applications. Additionally, the self-healing capability of the ionic hydrogel electrodes ensures reusability after mechanical damage. Figure 3(j) compares EMG signals from the ionic hydrogel in its normal state and after self-healing from damage. The results show negligible differences, indicating the ionic hydrogel's excellent reusability for electrophysiological monitoring applications. Further, the ionic hydrogel was attached to the thigh skin, the EMG signals were recorded under the static knee bending state and dynamic jumping state, as shown in Fig. S12 in the ESM. The ionic hydrogel can acquire both stable EMG signals under static knee bending and dynamic jumping state, demonstrating good dynamic stability of the ionic hydrogel in EMG signal acquisition.

### 2.4 CNN-assisted hand gesture recognition using ionic hydrogel electrodes array

The precise electrophysiological signal acquisition capability of ionic hydrogel electrodes makes them ideal for capturing EMG signals from hand injury patients. These EMG signals can be processed by a CNN to differentiate the subtle signal differences between diverse hand gestures, enabling the development of hand rehabilitation systems for hand injury patients when combined with VR HMIs. Firstly, a testing subject performed 14 task-oriented hand gestures according to the Jebsen hand function test. Figure 4(a) demonstrates the photographs of the 14 hand gestures, including resisted extension and flexion, resisted grip flexion, catching with palm, ball control with palm, stacking small objects, pinching cards, flipping cards, grasping a cup, transferring a cup, patting, tapping, inserting wooden pegs, twisting threaded screws, and drawing. For handling the problems of electrodes position shifts when donning and doffing the device between sessions, as well as comprehensively capturing detailed EMG signal information for a specific gesture, six channels of ionic hydrogel electrodes were used. Each channel consists of two testing electrodes and one reference electrode with the size of 10 mm × 10 mm. During EMG monitoring, the 12 testing electrodes were adhered around the forearm with the interval of 20 mm, while the six reference electrodes were adhered to the back of the hand. Five volunteers participated in the EMG signals acquisition, performing the 14 hand gestures to gather sufficient data for CNN training. For each gesture, 100 sets of EMG

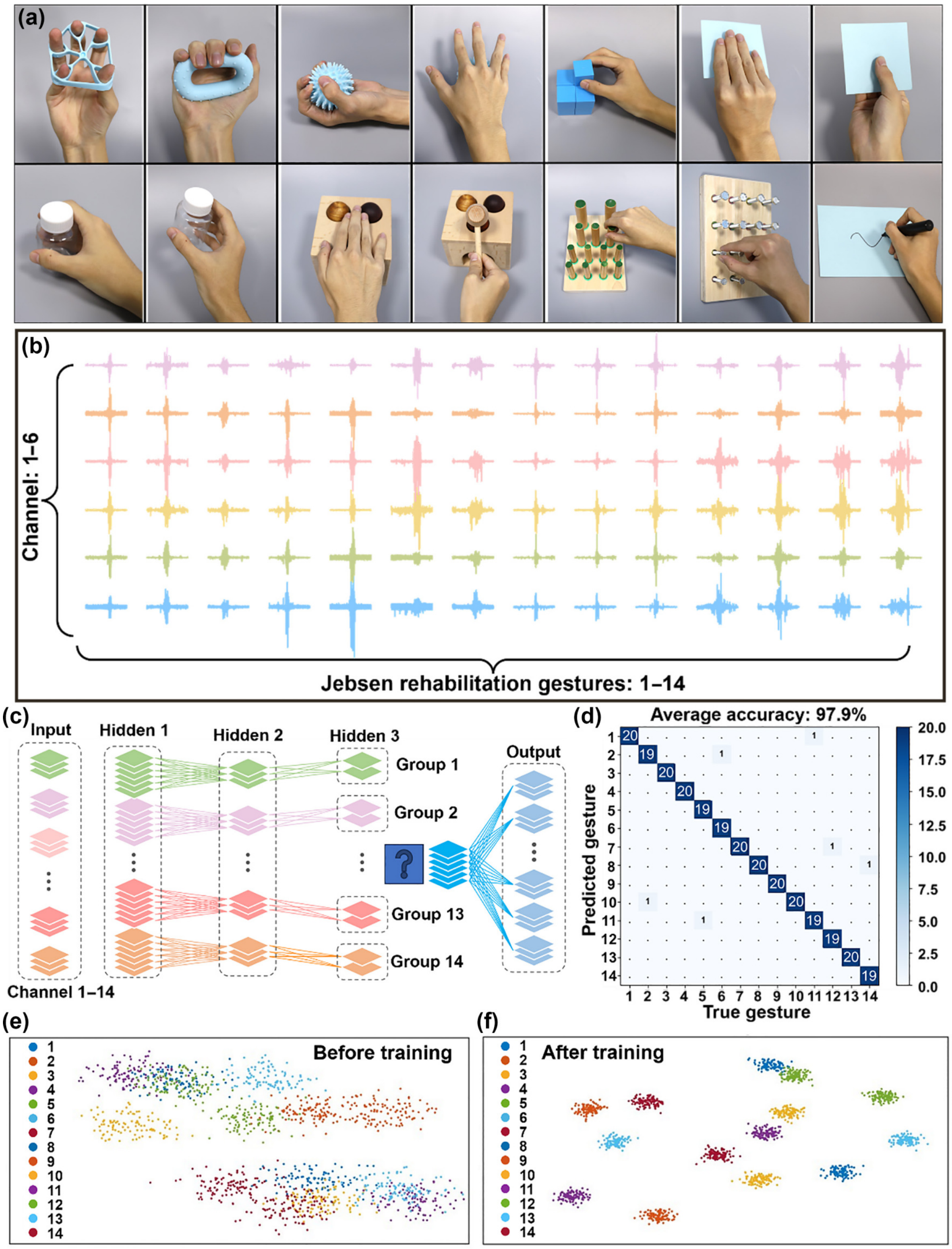


**Figure 4** CNN-assisted hand motion recognition using the ionic hydrogel electrodes array. (a) Photographs of 14 hand gestures according to the Jebsen hand function test. (b) 6-channel raw EMG signals of one volunteer for the 14 Jebsen hand gestures. (c) Schematic illustration for structure of the constructed CNN model. (d) Confusion matrix result for the CNN training of 5600 EMG signal data sets. (e) Distribution of the initial data before training in a 2D space. (f) Distribution of the datasets after training in a 2D space.

data were collected per volunteer, resulting in 7000 total sets of EMG signals. Figure 4(b) shows the 6-channel EMG signals for one of the volunteer's 14 Jebsen hand gestures, with additional EMG data for the other 4 volunteers provided in Figs. S13–S16 in the ESM. Notably, slight differences in signal patterns and intensities can be observed across the six channels for each hand gesture, and signal waveforms also varied between 14 different gestures. These differences are too complex and irregular to distinguish different gestures. So these 7000 sets of EMG data were submitted to a self-designed CNN model for training and improving hand gesture recognition accuracy. Figure 4(c) schematically illustrates the CNN structure, which consists of one input layer, three hidden layers, and one output layer. A total of 5600 EMG signal data sets were used for training, while 1400 EMG data sets were reserved for testing. Figure 4(d) shows the confusion matrix of the results. Each column of the matrix is the true gesture, and each row is the predicted gesture. It indicates that the average recognition accuracy for 14 hand gestures can reach up to 97.9%. To demonstrate the classification capability of the designed CNN model, a t-distributed Stochastic Neighbor Embedding (t-SNE) method was applied for visualizing all EMG data before and after CNN processing. Figure 4(e) presents the distribution of the original data before training using principal components 1 (PC1) and principal components 2 (PC2) axes in a two-dimensional (2D) space. The clusters with various colors stood for the datasets of different gestures. Initially, most of untrained datasets overlapped, making it difficult to distinguish between gestures. In contrast, Fig. 4(f) shows that after CNN processing, the datasets had clearer boundaries, showing enhanced intra-class compactness and greater inter-class separability. The above principal component analysis (PCA) results highlight the excellent classification capability of the constructed CNN in recognizing 14 Jebsen hand function gestures.

## 2.5 VR hand rehabilitation system for hand injury patients

Combining the high accuracy of CNN-assisted hand gesture recognition with VR HMIs, we further developed a VR hand rehabilitation system for patients suffering from hand injuries. Figure 5(a) illustrates the process flow of the hand rehabilitation system. The designed module primarily includes four key components: the EMG signal acquisition system, neural network training and prediction, signal communication module, and a VR display module developed in Unity. Participants in the rehabilitation program follow training instructions to perform specific hand gestures. The corresponding EMG signals are collected and processed by the trained neural network, which then

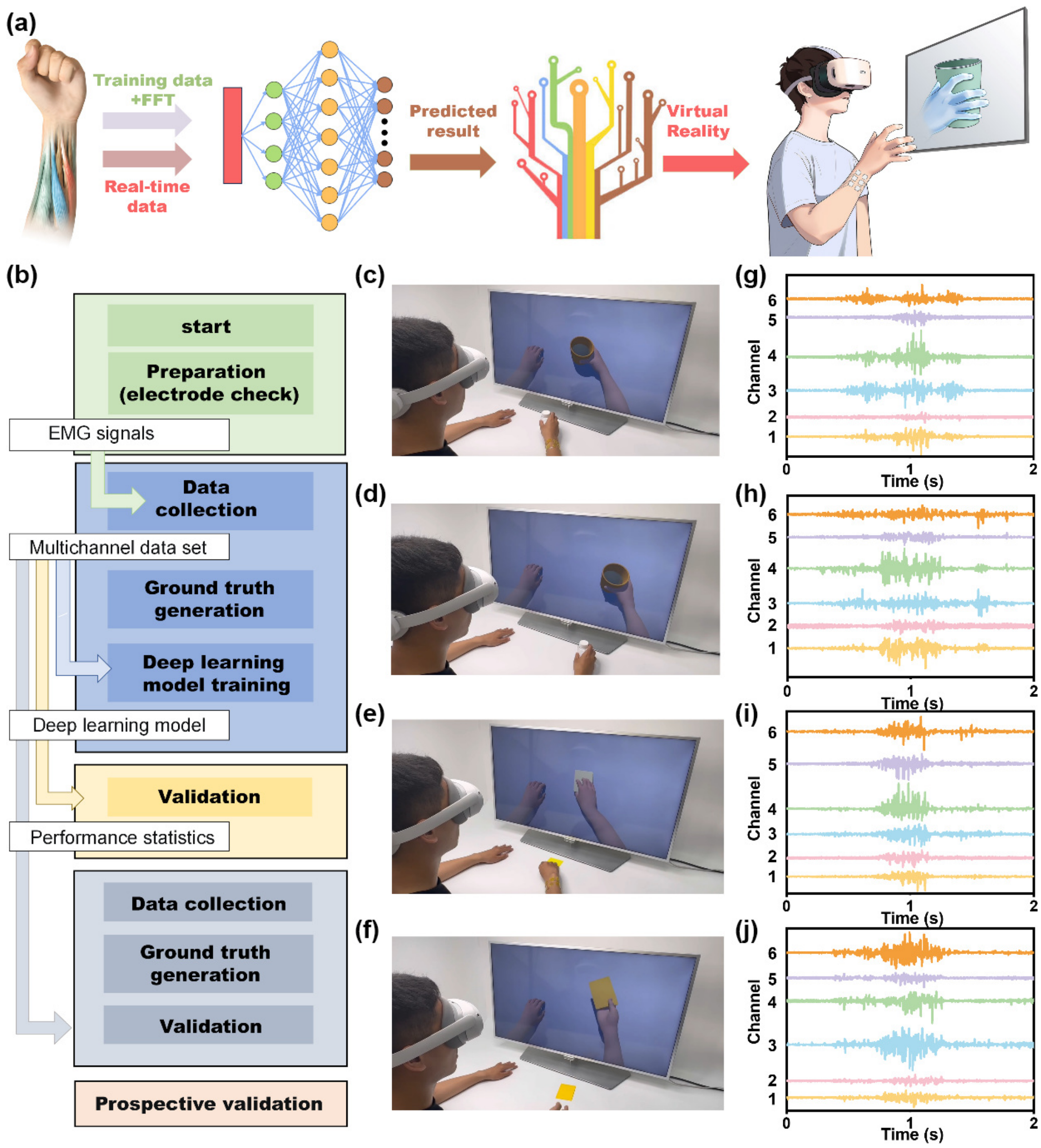


**Figure 5** VR hand rehabilitation system for hand injury patients. (a) Sketch illustrating the process flow of the VR hand rehabilitation system. (b) Overview of the logic of the EMG hand motion recognition assisted by the CNN model. (c)–(f) Photographs of a participant wearing a VR headset while performing the four hand motions including grasping a cup, moving a cup, pinching cards, and flipping cards. (g)–(j) 6-channel real-time EMG signals corresponding to the left four hand gestures.

accurately predicts the hand motions. Subsequently, the processor sends corresponding commands to Unity through a signal communication module. Upon receiving the signals, Unity displays the recognized hand gestures in real-time within the VR space. This process enables participants who wear a VR headset to interact with and receive feedback on their hand movements in a virtual space, achieving VR HMIs for rehabilitation purposes. Figure 5(b) provides an overview of the deep learning-assisted EMG recognition logic. The process starts with an inspection of the ionic hydrogel electrodes to allow proper adhesion to skin, assuring the accuracy and stability of the acquired signals. EMG signals are collected from six channels and organized into a dataset for training the neural network. Ground truth labels are generated for the collected data, referred to as "ground truth generation", to serve as benchmarks during training. A CNN was used to identify and classify EMG signals by learning patterns in the data, a process involving the collaboration of multiple convolutional layers, activation functions, pooling layers, and fully connected layers. After training, the model was validated on a separate dataset to evaluate the accuracy and generalization. This process was iterative, involving multiple rounds of data collection, validation, and optimization to enhance the model's effectiveness and reliability. To demonstrate the VR hand rehabilitation system's potential, we selected four typical hand motions for testing, including grasping a cup, moving a cup, pinching cards, and flipping cards. Figures 5(c)–5(f) demonstrate the photographs of a participant wearing a VR headset while performing the four hand motions. The 6-channel EMG signals corresponding to these motions were collected and transmitted to the CNN for motion recognition. Figures 5(g)–5(j) exhibit the 6 channels of real-time EMG signals corresponding to the hand motions in the left photograph. It can be seen from Figs. 5(c)–5(f) that the recognized hand gestures were successfully communicated with the VR Unity platform, which displayed the corresponding motions on the screen. The participant could see their hand motions replicated in real-time within the VR headset, providing instant feedback on their rehabilitation progress. The VR hand rehabilitation system has shown promising results, and a demonstration of the VR rehabilitation process can be found in Videos S1 and S2 in the ESM. This innovative approach to hand rehabilitation offers a dynamic and interactive environment for patients, enabling more engaging and precise recovery exercises.

## 3 Conclusions

In summary, we developed a non-hand-worn and load-free VR hand rehabilitation system through the combination of deep learning-assisted EMG recognition and VR HMIs. The EMG signals were acquired by a 6-channel stretchable ionic hydrogel electrode array, which was prepared by PEI/TA coacervate hydrogel and LiCl. The ionic hydrogel electrode exhibits superior conductivity, stretchability, wet adhesiveness, and self-healing abilities, enabling the ionic hydrogel to acquire reliable electrophysiological signals such as EMG, EEG, and ECG at both static and sports conditions. Assisted by a deep-learning CNN model, the ionic hydrogel electrode array can realize recognition of 14 Jebsen hand rehabilitation gestures with a high average accuracy reaching 97.9%. This EMG-based gesture recognition was further used to communicate with the Unity platform in the VR system to achieve immersive hand rehabilitation within the virtual space. Compared with current rehabilitation methods, the developed system can provide immersive task-oriented hand exercises in real-life scenarios without the need for hand-worn weights, as well as removing the constraints of time and location. This EMG-controlled VR rehabilitation system could bring great opportunities for the new generation of load-free, home-based immersive hand rehabilitation therapy.

## 4 Experimental section

### 4.1 Preparation of the ionic hydrogel

The branched PEI was added in deionized water with concentration of 10 wt.% and stirred thoroughly until fully dissolved. Different amounts of LiCl particles, the weight of the LiCl particles versus the volume of the PEI solution, were then added to the PEI solution, and the LiCl particles were stirred until completely dissolved. Subsequently, lipoic acid (TA) was added to the PEI solution. Due to the strong cohesive nature of lipoic acid, continuous stirring was required during the addition to prevent its self-coagulation. The mass ratio of TA to PEI was maintained at 1:5. The mixture solution was stirred for one minute before being poured into a pre-prepared mold and left to settle. The sample was then placed in a drying oven under 40 °C for 8 h, yielding an ion-conductive hydrogel with high conductivity and adhesiveness.

### 4.2 Characterization and measurement

The ionic hydrogel's mechanical properties were characterized using a Mark-10 mechanical testing system to obtain tensile stress–strain curves, with sample dimensions of 20 mm × 10 mm. Impedance tests were conducted using an electrochemical workstation (Zahner IM6) with two stainless steel electrodes sandwiching the samples. The AC impedance was tested from 4 MHz to 1 Hz with a 10 mV applied bias. The curve of adhesion force was measured by a lap-shear testing method on the Mark-10 tensile testing machine. The ionic hydrogels were adhered between various substrates with an adhesion area of 20 mm × 20 mm. When testing wet adhesion ability, the surfaces of the substrates were moistened by spraying water on the substrate followed by the same lap-shear test. For electrophysiological signal testing, ECG tests were conducted by using a heart and brain SpikerBox device (Backyard Brains), and EMG tests were recorded with a Muscle SpikerShield Pro toolkit. EEG tests were conducted using a biomedical signal acquisition system. To ensure accurate signal export, a copper tape was connected onto ionic hydrogel with the back covered with diaphragm in order to prevent interference from direct skin contact.

### 4.3 Deep-learning-based data analytics

To collect sufficient and comprehensive hand motion EMG data for training, data were collected from five volunteers performing 14 different hand gestures, with each gesture repeated 100 times. EMG signals were acquired using a six-channel ionic hydrogel electrode sensor. To ensure the diversity and applicability of the dataset, five volunteers were chosen with significant differences in gender, age, and body type. Subsequently, to guarantee data quality and consistency, ground truth labeled data corresponding to the collected signals were generated for comparison. To manage data complexity and storage, the data were down sampled by a factor of 100:1, and integration processing was used to convert the multi-channel dataset into a continuous data stream for subsequent analysis and model training. To construct a comprehensive and representative dataset, the normalized database corresponding to these 14 gestures was divided into two parts: 80% of the dataset was randomly selected as training samples, while the remaining 20% was reserved as a validation set. A CNN was constructed using the PyTorch framework, consisting of an input layer, multiple convolutional layers, pooling layers, fully connected layers, and an output layer. This CNN model was trained to extract features from the EMG data and perform gesture classification. During model training and validation, network parameters were optimized using the stochastic gradient descent (SGD) algorithm. The model's performance was evaluated using the validation set to ensure accurate gesture recognition and robustness in practical applications. The processing of data for real-time gesture recognition was conducted through a designed Python script, including filtering, sampling, integration, and normalization processes. The normalized database of Jebsen hand function gestures comprised 7000 datasets. These processes established a solid foundation for further research and practical applications of the EMG-based gesture recognition system.

**Electronic Supplementary Material**: Supplementary material (formation mechanism of the ionic hydrogel, contact impedance of ionic hydrogel, Young's Modulus of the ionic hydrogels, adhesion forces of the ionic hydrogel on porcine skin, adhesion force of the ionic hydrogel with different adhesion times, electrical impedance of the ionic hydrogel on porcine skin, extracted heart rate of consecutive ECG monitoring by the ionic hydrogel, detailed ECG waveform acquired by the ionic hydrogel, EMG signals acquired by the ionic hydrogel under static and dynamic state, and 6-channel raw EMG signals of 14 Jebson hand function gestures from other 4 volunteers) is available in the online version of this article at https://doi.org/10.26599/NR.2025.94907301.

## Data availability

All data needed to support the conclusions in the paper are presented in the manuscript and the Electronic Supplementary Material. Additional data related to this paper may be requested from the corresponding author upon request.

## Acknowledgments

This work was supported by the Scientific and Technological Project in Henan Province (No. 242102231002) and China Postdoctoral Science Foundation (No. 2022M712852).

## Declaration of competing interest

All the contributing authors report no conflict of interests in this work.

## Author contribution statement

P. C. Z.: Experimental design, writing manuscript. M. J. N.: Data curation, project administration, validation. S. Y. L.: Data curation, experimental design. W. Q. Y.: Experimental design. Y. T. Z.: Data curation. K. C.: Validation. Z. F. P.: Project administration. Y. C. M.: Project administration, experimental design, writing manuscript. All the authors have approved the final manuscript.

## Use of AI statement

None.

## References

[1] Powell, M. P.; Verma, N.; Sorensen, E.; Carranza, E.; Boos, A.; Fields, D. P.; Roy, S.; Ensel, S.; Barra, B.; Balzer, J. et al. Epidural stimulation of the cervical spinal cord for post-stroke upper-limb paresis. *Nat. Med.* **2023**, *29*, 689–699.

[2] Hunter, D. J.; Schofield, D.; Callander, E. The individual and socioeconomic impact of osteoarthritis. *Nat. Rev. Rheumatol.* **2014**, *10*, 437–441.

[3] Liu, Y.; Xie, W. C.; Tang, Z. B.; Tan, Z. F.; He, Y. Z.; Luo, J.; Wang, X. L. A reconfigurable integrated smart device for real-time monitoring and synergistic treatment of rheumatoid arthritis. *Sci. Adv.* **2024**, *10*, eadj0604.

[4] Li, T. F.; Zhao, H.; Li, H. F.; Zhang, Z. B.; Han, F.; Fang, P.; Li, G. L.; Xie, R. J.; Li, Q. S.; Gao, X. H. et al. Dual-modal stretchable sensing patches for *in situ* monitoring of electromyography and acoustic myography. *Adv. Funct. Mater.* **2024**, *34*, 2409780.

[5] Wang, H.; Ding, Q. L.; Luo, Y. B.; Wu, Z. X.; Yu, J. H.; Chen, H. Z.; Zhou, Y. B.; Zhang, H.; Tao, K.; Chen, X. L. et al. High-performance hydrogel sensors enabled multimodal and accurate human-machine interaction system for active rehabilitation. *Adv. Mater.* **2024**, *36*, 2309868.

[6] Luo, J. Z.; Li, Y. S.; He, M.; Wang, Z. M.; Li, C. Y.; Liu, D.; An, J.; Xie, W. Q.; He, Y. Q.; Xiao, W. F. et al. Rehabilitation of total knee arthroplasty by integrating conjoint isometric myodynamia and real-time rotation sensing system. *Adv. Sci.* **2022**, *9*, 2105219.

[7] Li, S. Y.; Liu, A. D.; Qiu, W.; Wang, Y. M.; Liu, G. Q.; Liu, J. R.; Shi, Y. T.; Li, Y. X.; Li, J. N.; Cai, W. J. et al. An all-protein multisensory highly bionic skin. *ACS Nano* **2024**, *18*, 4579–4589.

[8] Siviy, C.; Baker, L. M.; Quinlivan, B. T.; Porciuncula, F.; Swaminathan, K.; Awad, L. N.; Walsh, C. J. Opportunities and challenges in the development of exoskeletons for locomotor assistance. *Nat. Biomed. Eng.* **2023**, *7*, 456–472.

[9] Sui, M. L.; Ouyang, Y. M.; Jin, H.; Chai, Z. Y.; Wei, C. Y.; Li, J. Y.; Xu, M.; Li, W. H.; Wang, L.; Zhang, S. W. A soft-packaged and portable rehabilitation glove capable of closed-loop fine motor skills. *Nat. Mach. Intell.* **2023**, *5*, 1149–1160.

[10] Zhang, X. B.; Mo, X. Y.; Li, C. B.; Li, F. L.; Jin, J.; Xie, P.; Yao, G.; Lin, Y.; Yao, D. Z.; Xu, P. A wearable master-slave rehabilitation robot based on an epidermal array electrode sleeve and multichannel electromyography network. *Adv. Intell. Syst.* **2023**, *5*, 2200313.

[11] Ben-Tzvi, P.; Ma, Z. Sensing and force-feedback exoskeleton (SAFE) robotic glove. *IEEE Trans. Neural Syst. Rehabil. Eng.* **2015**, *23*, 992–1002.

[12] Han, Y. L.; Xu, Q.; Wu, F. Design of wearable hand rehabilitation glove with bionic fiber-reinforced actuator. *IEEE J. Transl. Eng. Health Med.* **2022**, *10*, 2100610.

[13] Tang, Z. C.; Wang, H.; Cui, Z. X.; Jin, X. N.; Zhang, L. K.; Peng, Y. X.; Xing, B. X. An upper-limb rehabilitation exoskeleton system controlled by MI recognition model with deep emphasized informative features in a VR scene. *IEEE Trans. Neural Syst. Rehabil. Eng.* **2023**, *31*, 4390–4401.

[14] Dragusanu, M.; Iqbal, M. Z.; Baldi, T. L.; Prattichizzo, D.; Malvezzi, M. Design, development, and control of a hand/wrist exoskeleton for rehabilitation and training. *IEEE Trans. Robot.* **2022**, *38*, 1472–1488.

[15] Verdel, D.; Bruneau, O.; Sahm, G.; Vignais, N.; Berret, B. The value of time in the invigoration of human movements when interacting with a robotic exoskeleton. *Sci. Adv.* **2023**, *9*, eadh9533.

[16] Tran, P.; Jeong, S.; Herrin, K. R.; Desai, J. P. Review: Hand exoskeleton systems, clinical rehabilitation practices, and future prospects. *IEEE Trans. Med. Robot. Bion.* **2021**, *3*, 606–622.

[17] Zhu, M. L.; Sun, Z. D.; Zhang, Z. X.; Shi, Q. F.; He, T. Y. Y.; Liu, H. C.; Chen, T.; Lee, C. Haptic-feedback smart glove as a creative human-machine interface (HMI) for virtual/augmented reality applications. *Sci. Adv.* **2020**, *6*, eaaz8693.
[18] Molinaro, D. D.; Kang, I.; Young, A. J. Estimating human joint moments unifies exoskeleton control, reducing user effort. *Sci. Robot.* **2024**, *9*, eadi8852.
[19] Chen, X. S.; Gong, L.; Wei, L.; Yeh, S. C.; Xu, L. D.; Zheng, L. R.; Zou, Z. A wearable hand rehabilitation system with soft gloves. *IEEE Trans. Ind. Informat.* **2021**, *17*, 943–952.
[20] Gao, S.; He, T. Y. Y.; Zhang, Z. X.; Ao, H. R.; Jiang, H. Y.; Lee, C. A motion capturing and energy harvesting hybridized lower-limb system for rehabilitation and sports applications. *Adv. Sci.* **2021**, *8*, 2101834.
[21] Kim, J. J.; Wang, Y.; Wang, H. Y.; Lee, S.; Yokota, T.; Someya, T. Skin electronics: Next-generation device platform for virtual and augmented reality. *Adv. Funct. Mater.* **2021**, *31*, 2009602.
[22] Amin, F.; Waris, A.; Syed, S.; Amjad, I.; Umar, M.; Iqbal, J.; Omer Gilani, S. Effectiveness of immersive virtual reality-based hand rehabilitation games for improving hand motor functions in subacute stroke patients. *IEEE Trans. Neural Syst. Rehabil. Eng.* **2024**, *32*, 2060–2069.
[23] Huang, Y.; Zhou, J. K.; Ke, P. C.; Guo, X.; Yiu, C. K.; Yao, K. M.; Cai, S. Y.; Li, D. F.; Zhou, Y.; Li, J. et al. A skin-integrated multimodal haptic interface for immersive tactile feedback. *Nat. Electron.* **2023**, *6*, 1020–1031.
[24] Xiao, X.; Fang, Y. S.; Xiao, X.; Xu, J.; Chen, J. Machine-learning-aided self-powered assistive physical therapy devices. *ACS Nano* **2021**, *15*, 18633–18646.
[25] Jha, C. K.; Shukla, Y.; Mukherjee, R.; Rathva, P.; Joshi, M.; Jain, D. A glove-based virtual hand rehabilitation system for patients with post-traumatic hand injuries. *IEEE Trans. Biomed. Eng.* **2024**, *71*, 2033–2041.
[26] Oh, J.; Kim, S.; Lee, S.; Jeong, S.; Ko, S. H.; Bae, J. A liquid metal based multimodal sensor and haptic feedback device for thermal and tactile sensation generation in virtual reality. *Adv. Funct. Mater.* **2021**, *31*, 2007772.
[27] Zhu, M. L.; Sun, Z. D.; Lee, C. Soft modular glove with multimodal sensing and augmented haptic feedback enabled by materials' multifunctionalities. *ACS Nano* **2022**, *16*, 14097–14110.
[28] Yang, S. J.; Cheng, J. H.; Shang, J.; Hang, C.; Qi, J.; Zhong, L. N.; Rao, Q. Y.; He, L.; Liu, C. Q.; Ding, L. et al. Stretchable surface electromyography electrode array patch for tendon location and muscle injury prevention. *Nat. Commun.* **2023**, *14*, 6494.
[29] Kumar, D. K.; Pah, N. D.; Bradley, A. Wavelet analysis of surface electromyography. *IEEE Trans. Neural Syst. Rehabil. Eng.* **2003**, *11*, 400–406.
[30] Lin, Y.; Li, Q. S.; Ding, C.; Wang, J. Y.; Yuan, W.; Liu, Z. Y.; Su, W. M.; Cui, Z. High-resolution and large-size stretchable electrodes based on patterned silver nanowires composites. *Nano Res.* **2022**, *15*, 4590–4598.
[31] Zhao, Q. N.; Gribkova, E.; Shen, Y. Y.; Cui, J. L.; Naughton, N.; Liu, L. S.; Seo, J.; Tong, B. X.; Gazzola, M.; Gillette, R. et al. Highly stretchable and customizable microneedle electrode arrays for intramuscular electromyography. *Sci. Adv.* **2024**, *10*, eadn7202.
[32] Jeon, J.; Park, J. W. Stretchable electrodes for interconnects in soft electronics. *Nano Lett.* **2024**, *24*, 9553–9560.
[33] Farina, D.; Jiang, N.; Rehbaum, H.; Holobar, A.; Graimann, B.; Dietl, H.; Aszmann, O. C. The extraction of neural information from the surface EMG for the control of upper-limb prostheses: Emerging avenues and challenges. *IEEE Trans. Neural Syst. Rehabil. Eng.* **2014**, *22*, 797–809.
[34] Zhang, Q.; Lambeth, K.; Sun, Z. Y.; Dodson, A.; Bao, X. F.; Sharma, N. Evaluation of a fused sonomyography and electromyography-based control on a cable-driven ankle exoskeleton. *IEEE Trans. Robot.* **2023**, *39*, 2183–2202.
[35] Wang, S. Y.; Wang, X.; Zhang, W. F.; Shi, X. H.; Song, D. K.; Zhang, Y.; Zhao, Y.; Zhao, Z. H.; Liu, N. Electronic tattoos based on large-area $Mo_2C$ grown by chemical vapor deposition for electrophysiology. *Nano Res.* **2023**, *16*, 4100–4106.
[36] LeCun, Y.; Bengio, Y.; Hinton, G. Deep learning. *Nature* **2015**, *521*, 436–444.
[37] Wainberg, M.; Merico, D.; Delong, A.; Frey, B. J. Deep learning in biomedicine. *Nat. Biotechnol.* **2018**, *36*, 829–838.
[38] Ran, X.; Luo, F. Y.; Lin, Z. M.; Zhu, Z. Y.; Liu, C. J.; Chen, B. Blood pressure monitoring via double sandwich-structured triboelectric sensors and deep learning models. *Nano Res.* **2022**, *15*, 5500–5509.
[39] Li, N.; Wang, Z. S.; Yang, X. R.; Zhang, Z. Y.; Zhang, W. D.; Sang, S. B.; Zhang, H. L. Deep-learning-assisted thermogalvanic hydrogel e-skin for self-powered signature recognition and biometric authentication. *Adv. Funct. Mater.* **2024**, *34*, 2314419.
[40] Fang, Y. S.; Xu, J.; Xiao, X.; Zou, Y. J.; Zhao, X.; Zhou, Y. H.; Chen, J. A deep-learning-assisted on-mask sensor network for adaptive respiratory monitoring. *Adv. Mater.* **2022**, *34*, 2200252.
[41] Liu, Y.; Li, C.; Yu, L. X.; Wu, Z. W.; Fan, S. C.; Lv, R. T. Ultra-high sensitivity fiber optic microphone with corrugated graphene-oxide diaphragm for voice recognition. *Nano Res.* **2024**, *17*, 7593–7602.
[42] Zhang, P. P.; Guo, W. B.; Guo, Z. H.; Ma, Y.; Gao, L.; Cong, Z. F.; Zhao, X. J.; Qiao, L. J.; Pu, X.; Wang, Z. L. Dynamically crosslinked dry ion-conducting elastomers for soft iontronics. *Adv. Mater.* **2021**, *33*, 2101396.
[43] Ding, H. Y.; Liang, X. X.; Wang, Q.; Wang, M. M.; Li, Z. J.; Sun, G. X. A semi-interpenetrating network ionic composite hydrogel with low modulus, fast self-recoverability and high conductivity as flexible sensor. *Carbohydr. Polym.* **2020**, *248*, 116797.
[44] Kong, B.; Liu, R.; Hu, X. J.; Li, M. Y.; Zhou, X. T.; Zhao, Y. J.; Kong, T. T. Cornea-inspired ultrasound-responsive adhesive hydrogel patches for keratitis treatment. *Adv. Funct. Mater.* **2024**, *34*, 2310544.
[45] Zhang, J.; Chen, X. M.; Lin, J. S.; Zhang, P.; Lei, I. M.; Tao, Y.; Zhang, J. J.; Luo, T.; Liu, J. Hydrogel bioadhesives harnessing nanoscale phase separation for Achilles tendon repairing. *Nano Res.* **2024**, *17*, 778–787.
[46] Yang, C. C.; Ji, C. C.; Guo, F. J.; Mi, H. Y.; Wang, Y. W.; Qiu, J. S. Wireless sensor system based on organohydrogel ionic skin for physiological activity monitoring. *ACS Appl. Mater. Interfaces* **2024**, *16*, 25181–25193.
[47] Wang, S. H.; Wang, Z. M.; Zhang, L.; Song, Z. Q.; Liu, H.; Xu, X. Sweat-adaptive adhesive hydrogel electronics enabled by dynamic hydrogen bond networks. *Chem. Eng. J.* **2024**, *492*, 152290.
[48] Li, X.; Zhu, P. C.; Zhang, S. C.; Wang, X. C.; Luo, X. P.; Leng, Z. W.; Zhou, H.; Pan, Z. F.; Mao, Y. C. A self-supporting, conductor-exposing, stretchable, ultrathin, and recyclable kirigami-structured liquid metal paper for multifunctional e-skin. *ACS Nano* **2022**, *16*, 5909–5919.
[49] Leng, Z. W.; Zhu, P. C.; Wang, X. C.; Wang, Y. F.; Li, P. S.; Huang, W.; Li, B. C.; Jin, R.; Han, N. N.; Wu, J. et al. Sebum-membrane-inspired protein-based bioprotonic hydrogel for artificial skin and human-machine merging interface. *Adv. Funct. Mater.* **2023**, *33*, 2211056.
[50] Li, Y.; Gu, Y. Z.; Qian, S.; Zheng, S. W.; Pang, Y. C.; Wang, L. L.; Liu, B. G.; Liu, S. J.; Zhao, Q. An injectable, self-healable, and reusable PEDOT:PSS/PVA hydrogel patch electrode for epidermal electronics. *Nano Res.* **2024**, *17*, 5479–5490.
[51] Xu, Y. D.; Zhao, G. G.; Zhu, L.; Fei, Q. H.; Zhang, Z.; Chen, Z. Y.; An, F. F.; Chen, Y. Y.; Ling, Y.; Guo, P. J. et al. Pencil-paper on-skin electronics. *Proc. Natl. Acad. Sci. USA* **2020**, *117*, 18292–18301.